Nonlinear Modelling Of Ultrafast Free-Electron Dynamics and Transient Reflectivity in Water-Like Media under Femtosecond Laser Excitation

VIOLETA PETROVIĆ[1], HRISTINA DELIBAŠIĆ MARKOVIĆ[1], IVAN PETROVIĆ[2]
[1] Faculty of Science, University of Kragujevac,
Radoja Domanovića 12, 34000 Kragujevac,
SERBIA

[2] Department in Kragujevac,
Academy of Professional Studies Šumadija,
Kosovska 8, 34000 Kragujevac,
SERBIA

Abstract: - Ultrafast laser excitation of transparent dielectric media initiates a sequence of electronic processes that determine the early stages of energy deposition and the resulting optical response. We investigate the generation and temporal evolution of free carriers in water-like dielectric media irradiated by femtosecond laser pulses. The carrier dynamics are described within a nonlinear rate-equation framework, while the resulting time-dependent electron density is used to evaluate the transient optical response through a Drude-type dielectric function and Fresnel relations. The analysis reveals a pronounced wavelength dependence of the carrier generation efficiency arising from the variation of the multiphoton excitation order across the considered spectral range. We have shown that wavelength-dependent nonlinear excitation governs both the buildup of free carriers and the resulting ultrafast optical response, providing a consistent framework for interpreting pump-probe reflectivity measurements in water-like dielectric systems.

Key-Words: - Ultrafast laser-matter interaction, multiphoton ionization, avalanche ionization, free-carrier dynamics, transient reflectivity, Drude model, water-like dielectric media, pump-probe spectroscopy.

Received: March 17, 2025. Revised: August 22, 2025. Accepted: March 9, 2026. Published: July 13, 2026.

1 Introduction

The interaction of intense ultrafast laser pulses with transparent dielectric media has attracted considerable attention over the past decades, [1], [2]. In wide-bandgap materials, femtosecond laser excitation drives electronic transitions on sub-picosecond timescales, long before significant thermal diffusion, acoustic relaxation, or structural modification can occur. As a result, the early stage of the interaction is governed primarily by purely electronic processes, leading to the rapid excitation of electrons from the valence band into the conduction band. The resulting generation of free carriers represents the initial stage of laser-induced breakdown (LIB) and strongly modifies the transient optical properties of the medium. Because these processes occur before the onset of significant thermal or mechanical effects, femtosecond excitation enables highly localized and controlled interaction with matter, which underlies applications in precision material processing and biomedical photonics, [3], [4].

In transparent and weakly absorbing materials, the generation of conduction-band electrons during femtosecond irradiation occurs predominantly through nonlinear photoionization (PI) mechanisms. Depending on the strength of the optical field, PI may proceed via multiphoton absorption or tunnelling ionization (TI), while the initially produced carriers can subsequently initiate avalanche multiplication through impact ionization, [5]. The interplay between these processes determines the temporal evolution of the electron population during the laser pulse and ultimately governs whether the material remains weakly perturbed or evolves toward a dense plasma-like state. The efficiency of nonlinear PI depends strongly on the excitation wavelength and the bandgap of the material, which together determine the number of photons required for carrier generation and the probability of electron excitation.

A detailed understanding of this early electronic stage is essential for interpreting ultrafast optical measurements. Experimental studies commonly employ time-resolved pump-probe techniques to monitor transient changes in reflectivity or transmission induced by femtosecond excitation, [6], [7], [8]. These measurements provide direct insight into the evolution of the free-electron population and the associated modification of the dielectric function on sub-picosecond timescales. However, interpreting such signals requires theoretical models capable of linking the microscopic carrier-generation dynamics with the macroscopic optical response of the medium. Among the available theoretical approaches, rate-equation models have proven particularly useful for describing ultrafast carrier dynamics in laser-excited dielectrics, [9], [10]. When combined with optical response models based on the free-carrier contribution to the dielectric function, these approaches allow the calculated electron density to be directly related to experimentally observable quantities such as transient reflectivity or transmission.

Biological and aqueous materials provide a particularly interesting context for studies of ultrafast laser-matter interaction, [4]. A large fraction of biological matter consists of water, and many such systems exhibit optical properties similar to those of wide-bandgap dielectrics in the visible and near-infrared spectral regions. In the present work, the term water-like dielectric media refers to transparent materials whose refractive index and bandgap are comparable to those of liquid water ($n \approx 1.33, E_g \approx 6-7$ eV), [11]. The term is used here in an effective sense, referring to homogeneous dielectric systems with optical properties comparable to water, while neglecting additional complexities such as impurities and structural inhomogeneities that may influence the dynamics in real systems. Under femtosecond excitation, such media exhibit nonlinear ionization dynamics similar to those observed in conventional dielectric materials, where multiphoton excitation and subsequent carrier multiplication govern the initial stages of energy deposition. Understanding how these ultrafast electronic processes modify the optical response of water-like media is therefore essential both for interpreting pump-probe experiments and for improving laser-based biomedical techniques that rely on controlled microscopic energy deposition.

In this work, we investigate the ultrafast generation and evolution of free carriers in water-like dielectric media irradiated by femtosecond laser pulses. Pulse durations in the range of 50-100 fs and wavelengths spanning the visible to near-infrared region (400-1550 nm) are considered. The carrier dynamics are described using a nonlinear rate-equation model that includes multiphoton ionization (MPI), avalanche ionization (AI), and carrier recombination. The resulting time-dependent electron density is then used to calculate the transient optical response of the medium through a Drude-type dielectric function combined with Fresnel relations at normal incidence. This approach enables a direct connection between the microscopic ionization dynamics and the transient reflectivity signals observed in [12], [13].

The remainder of this paper is organized as follows. Section 2 presents the theoretical framework used to model the carrier dynamics and the corresponding optical response. Section 3 discusses the numerical results obtained for different excitation conditions and analyses the dependence of the electron density and transient reflectivity on the pulse parameters. Section 4 summarizes the main conclusions of the study.

2 Theoretical Framework

When a femtosecond laser pulse interacts with a transparent water-like dielectric medium, the earliest stage of the interaction is governed exclusively by ultrafast electronic processes. The strong optical field promotes bound electrons into the conduction band on sub-picosecond timescales, well before any significant lattice heating, heat diffusion, or mechanical relaxation develops. This separation of timescales is justified by the condition $\tau_p \ll \tau_{e-ph}$, where τ_p denotes the pulse duration and τ_{e-ph} the characteristic electron-phonon relaxation time. Under these conditions, the lattice remains effectively frozen during the optical excitation, so that thermal diffusion and structural relaxation can be neglected on the timescale of carrier generation. In this regime, the material response is determined entirely by electronic excitation, and the key dynamical quantity is the time-dependent free electron density $N_e(t)$, which controls the transient optical properties of the medium, [3], [14].

In wide-bandgap dielectric media, conduction-band electrons are initially generated by PI, which can proceed through MPI or TI. The relative importance of these mechanisms is rigorously determined by the Keldysh parameter, $\gamma = \omega\sqrt{2mE_g}/eE$, which distinguishes between the perturbative MPI regime ($\gamma \gg 1$) and the quasi-static tunnelling regime ($\gamma \ll 1$), [15], [16]. For the near-infrared excitation conditions considered here (intensities $I \sim 10^{12}$–10^{14} W cm^{-2} and photon

energies $\hbar\omega \approx 0.8$–3.1 eV), the corresponding field amplitudes yield $\gamma \approx 3$–15, placing the system unambiguously in the multiphoton regime. Representative values are obtained as $\gamma \approx 14.8$, 7.4, 5.8, and 3.8 for 400, 800, 1030, and 1550 nm at $I = 10^{12}$ W cm^{-2}, confirming the multiphoton character of the excitation. At higher peak intensities, γ approaches unity, and the MPI term is therefore interpreted as an effective PI source capturing the dominant wavelength dependence through the photon order K. Under these conditions, excitation remains dominated by nonlinear PI processes, with the lower-intensity part of the parameter range corresponding to a clear multiphoton regime and the highest intensities approaching the intermediate Keldysh range. Therefore, the PI source is described here by an effective K-photon MPI term, which retains the dominant wavelength dependence through the photon order K. This reduced description is appropriate for the present rate-equation model, whose main aim is to analyse the coupled evolution of carrier density, avalanche multiplication, and transient optical response. Within this framework, ionization occurs when a bound electron absorbs K photons whose combined energy exceeds the effective ionization threshold. This threshold consists of the bandgap E_g and the ponderomotive potential U_p, the latter representing the cycle-averaged quiver energy acquired by an electron in the oscillating optical field. The minimum photon number is therefore:

$$K = \langle \frac{E_g + U_p}{\hbar\omega} \rangle, \quad (1)$$

where ω denotes the angular frequency of the laser and $\hbar$ is the reduced Planck constant. The ponderomotive potential can be expressed as:

$$U_p = \frac{e^2 E^2}{4m\omega^2}, \quad (2)$$

or, in an approximate form, $U_p[\text{eV}] \approx 9.33 \times 10^{-14} I[\text{W cm}^{-2}]\lambda^2[\mu\text{m}^2]$. Because U_p increases with both intensity and wavelength, it raises the effective ionization threshold at longer wavelengths. However, for the moderate intensities used here, $U_p \ll E_g$, allowing the approximation $K \approx \langle E_g/\hbar\omega \rangle$, which simplifies the modelling while remaining accurate within the MPI regime. For the considered intensity range, $I \sim 10^{12}$–10^{14} W cm^{-2}, and wavelengths $\lambda = 400$–1550 nm, the U_p remains in the sub-eV range ($U_p \lesssim 0.1$–0.5 eV), i.e., at least one order of magnitude smaller than the bandgap energy ($E_g \approx 6$–7 eV). Consequently, the inclusion of U_p modifies the effective threshold only weakly, and the resulting variation in K does not exceed one photon across the spectral range investigated. This refined justification, which is based on the Keldysh criterion, numerical evaluation of γ, and comparison of ponderomotive and bandgap energies, ensures that the exclusive use of MPI is physically and mathematically consistent with the excitation conditions of the present study.

Since the effective ionization threshold is determined by both the bandgap and the ponderomotive energy, the probability of PI becomes highly sensitive to variations in the instantaneous laser intensity. In the perturbative regime identified above, $\gamma \gg 1$, the electron-field interaction is well described by a coherent K-photon transition, leading to an ionization rate that scales strongly with the field amplitude. The resulting MPI rate is therefore expressed in the standard form:

$$W_{MPI}(I) = \sigma_K I^K. \quad (3)$$

where σ_K denotes the generalized K-photon absorption coefficient associated with the relevant virtual transitions and the electronic structure of the medium. For water-like dielectric media, the magnitude of σ_K can be constrained using experimental observations from nonlinear spectroscopy and multiphoton microscopy, where similar excitation pathways are dominant, [14], [17]. Because the photon order for near-infrared excitation of wide-bandgap dielectrics typically lies in the range $K \sim 3$–8, the multiphoton rate exhibits an exceptionally steep intensity dependence. Therefore, $W_{\text{MPI}}(I) \propto I^K$ becomes highly localized in time, with the vast majority of conduction-band electrons generated in a narrow temporal window around the peak of the femtosecond pulse. Even the smallest variations in peak intensity arising from energy fluctuations or nonlinear propagation can therefore lead to orders-of-magnitude changes in the produced electron density. This extreme sensitivity is characteristic of the intrinsically nonlinear and threshold-like nature of multiphoton excitation. The electrons produced through MPI represent the seed population required to initiate subsequent carrier-multiplication mechanisms. Once a nonzero conduction-band density is established, these carriers may gain additional energy from the driving field and trigger impact-ionization events, giving rise to AI growth. Thus, the MPI process not only governs the initial carrier injection but also determines the temporal onset and efficiency of the nonlinear amplification dynamics that follow.

Once a seed population of conduction-band electrons has been produced through multiphoton excitation, additional carriers may be generated through avalanche (impact) ionization. In this secondary process, conduction-band electrons

acquire kinetic energy from the oscillating optical field between successive collisions. During electron-phonon or electron-impurity scattering events, part of this acquired energy may be transferred to a bound electron. When the transferred energy exceeds the impact-ionization threshold (typically comparable to the bandgap energy E_g), a new conduction-band electron is created. Repetition of these events leads to a cascade-like multiplication of carriers. This mechanism exhibits the same mathematical structure as classical Townsend amplification in gases, where the electron-impact ionization coefficient α_T depends exponentially on the ratio of threshold energy to the energy gained between collisions. In condensed dielectrics, similar reasoning leads to an effective ionization coefficient that increases with intensity and decreases with increasing scattering rate. A commonly used phenomenological representation for the avalanche contribution is:

$$W_{AI}(I, N_e) = \alpha I N_e, \quad (4)$$

where N_e denotes the instantaneous free-electron density, and α is the avalanche coefficient. The dependence on both I and N_e captures, respectively, the rate at which electrons acquire kinetic energy from the field and the multiplicative nature of the cascade. The coefficient α is, in general, intensity-dependent through microscopic transport processes; here, it is treated as an effective parameter evaluated at the characteristic intensity scale I_0, consistent with the nondimensional formulation where the temporal variation is captured by $\tilde{I}(\tau)$. The parameters are treated within an effective framework, with values constrained by literature, reflecting average microscopic processes and enabling a consistent description of the dominant ultrafast dynamics. In addition, the coefficient α subsumes microscopic transport parameters, including the electron-phonon collision frequency, the mean free path, and the critical energy E_g necessary for impact ionization, [3], [10]. In analogy with Townsend theory, α increases approximately as $\alpha \propto \exp[-E_g/\Delta E(I)]$, where $\Delta E(I)$ is the cycle-averaged kinetic energy acquired between collisions, which itself grows monotonically with the field amplitude. The multiplicative N_e dependence in Eq. (4) introduces a nonlinear positive feedback mechanism into the carrier dynamics. A simple linear-stability consideration shows that avalanche growth becomes self-sustaining when: $\alpha I > \tau_{\text{eff}}^{-1}$, where τ_{eff} is the effective electron lifetime determined by recombination and trapping. When this condition is satisfied, the AI term dominates over carrier-loss mechanisms, and the electron population exhibits exponential growth on sub-picosecond timescales. Otherwise, when $\alpha I < \tau_{\text{eff}}^{-1}$, AI contributions remain subcritical and do not significantly amplify the seed population. This threshold behaviour is a defining feature of impact ionization in dielectrics and explains the rapid growth of electron density that may occur even within a small fraction of the femtosecond pulse duration. Because both α and $I(t)$ vary temporally during the pulse, the onset of avalanche growth is confined to a temporal region close to the maximum of the pulse envelope. Under such conditions, the electron density can evolve from a weakly ionized state to a high-density plasma regime within tens of femtoseconds, provided that the seed population generated through multiphoton excitation is sufficient to trigger the avalanche feedback.

The joint action of MPI and avalanche growth governs the temporal evolution of the conduction-band electron density during ultrafast excitation. In addition to these generation channels, carriers are depleted through recombination and trapping, which can be incorporated into an effective recombination time τ_r. Under these assumptions, the electron density obeys the nonlinear rate equation:

$$\frac{dN_e}{dt} = \sigma_K I(t)^K + \alpha I(t) N_e - \frac{N_e}{\tau_r}, \quad (5)$$

revealing the competition between a high-order multiphoton source, a density-dependent avalanche term, and recombination losses. To expose the nonlinear structure of this equation, it is convenient to express the dynamics in nondimensional form by introducing the normalized density $n = N_e/N_c$, where N_c is the critical plasma density at the probe frequency, and the rescaled time variable $\tau = t/\tau_p$. With the Gaussian pulse envelope written as $I(t) = I_0 \exp[-4\ln 2\,(t/\tau_p)^2] = I_0\,\tilde{I}(\tau)$, the normalized intensity is defined as $\tilde{I}(\tau) = \exp[-4\ln 2\tau^2]$. The governing equation then becomes:

$$\frac{dn}{d\tau} = B\,\tilde{I}(\tau)^K + A\,\tilde{I}(\tau)\,n - \rho\,n, \quad (6)$$

where the dimensionless parameters $A = \alpha I_0 \tau_p$, $B = \sigma_K I_0^K \tau_p / N_c$, and $\rho = \tau_p/\tau_r$ characterize, respectively, the strength of avalanche amplification, multiphoton seeding, and carrier loss relative to the pulse duration. This form follows from the substitutions $N_e = nN_c$ and $t = \tau\tau_p$ in Eq. (5), which introduces I_0 and τ_p as the characteristic intensity and time scales of the problem. Within this scaling, the avalanche term $\alpha I(t) N_e$ reduces to $A\tilde{I}(\tau)n$, indicating that A represents the characteristic avalanche growth relative to the pulse timescale, while B quantifies the efficiency of multiphoton seeding with respect to the critical density. The coefficients α and σ_K are thus interpreted as effective parameters defined at the

reference intensity scale, whereas the temporal variation of the excitation is fully captured by the normalized envelope $\tilde{I}(\tau)$. The presented compact form (Eq. (6)) highlights the dynamical roles of each process: the MPI term establishes the initial seed density; the avalanche term introduces multiplicative feedback; and recombination provides a linear decay channel. The condition $A\,\tilde{I}(\tau) > \rho$ defines the instantaneous threshold for self-sustained avalanche growth. Below this threshold, the electron density relaxes toward zero, whereas above it, the system exhibits exponential growth until limited by pulse duration or depletion mechanisms. Because $\tilde{I}(\tau)$ is sharply peaked around $\tau = 0$, this threshold can be surpassed only within a narrow temporal interval near the pulse maximum, ensuring that the rapid rise of $n(\tau)$ occurs on tens-of-femtoseconds timescales. Consequently, the combined effect of the highly localized MPI source and the intensity-dependent avalanche gain leads to the characteristic sharply asymmetric temporal buildup of the free-electron population, ultimately driving the transition from a weakly perturbed dielectric to a dense plasma-like state during femtosecond excitation. Moreover, the appearance of N_c in the normalized density, $n = N_e/N_c$, naturally highlights its physical significance. The critical plasma density, N_c, is defined as the carrier concentration at which the plasma frequency equals the probing angular frequency, and within the Drude formalism is given by: $N_c = \varepsilon_0 m^* \omega^2 / e^2$. Since $\omega = 2\pi c/\lambda$, the critical density scales inversely with the square of the probe wavelength, implying that longer wavelengths require much lower electron densities to drive the material into a plasma-like optical state. As the simulated electron density approaches or exceeds N_c, the dielectric function undergoes strong modification, and the reflectivity increases sharply. Thus, comparing the evolving carrier density $N_e(t)$ with the critical density N_c provides a direct physical criterion for identifying the onset of strong optical perturbation during ultrafast excitation. Finally, it should be noted that the present approach is based on a mean-field description and neglects spatial inhomogeneities, carrier-carrier correlations, and nonlocal transport effects. Accordingly, the model is expected to remain valid primarily in the weak-to-moderate excitation regime, $N_e \ll N_c$, while deviations may arise as the carrier density approaches the critical plasma density.

The nondimensionalized form of the rate equation makes clear that the temporal evolution of the conduction-band population is governed by a balance between nonlinear generation, avalanche amplification, and carrier loss. Since the free-electron density evolves on the same ultrafast timescale as the driving field, the resulting $N_e(t)$ profile captures the complete electronic response of the medium during excitation. Importantly, the accumulation of carriers not only modifies the internal electron dynamics but also alters the macroscopic optical properties of the dielectric. Because the dielectric function of a wide-bandgap medium is highly sensitive to the presence of conduction-band electrons, even the smallest increases in $N_e(t)$ can produce measurable changes in reflectivity and transmission. When the electron density approaches a significant fraction of the critical plasma density N_c, the optical response transitions from dielectric-like to plasma-like. For this reason, the time-dependent electron density obtained from Eq. (6) serves as the fundamental input for modeling the transient optical behaviour of the laser-excited medium, motivating a Drude-based description of the dielectric response.

The temporal evolution of the free-electron density, determined by the coupled MPI and AI processes under the finite pulse envelope, directly governs the ultrafast optical response of the medium. As the conduction-band population increases, the electronic structure of the dielectric is modified on femtosecond timescales, producing measurable changes in macroscopic observables such as reflectivity. To describe this behaviour, the dielectric response of the excited medium is modelled within the Drude framework, which provides an effective plasma-like description of the free-carrier contribution to the permittivity, [10], [18]. Within this approximation, the time-dependent dielectric function is:

$$\varepsilon(\omega, t) = \varepsilon_b(\omega) - \frac{N_e(t)e^2}{\varepsilon_0 m^*} \cdot \frac{1}{\omega^2 + i\nu\omega}, \qquad (7)$$

where $\varepsilon_b(\omega)$ denotes the background permittivity of the unperturbed medium, m^* is the effective electron mass, taken equal to the free electron mass within the present Drude-type approximation, and ν is the collision frequency describing carrier-phonon and carrier-defect scattering. In the present model, ν parameter is treated as an effective constant parameter representing the average carrier scattering rate in water-like media. Experimental and theoretical studies typically place this quantity in the range 10^{14}–10^{15} s^{-1} for femtosecond laser excitation, which is adopted here as a reasonable order-of-magnitude estimate, [3], [10]. As the free-electron density grows, this contribution substantially modifies both the real and imaginary parts of the dielectric function, eventually driving the material toward a plasma-like regime. The strength

of this modification is governed by the ratio $N_e(t)/N_c$, where N_c is the critical plasma density introduced earlier. As $N_e(t)$ approaches a significant fraction of N_c, the real part of the dielectric function decreases toward zero and the reflectivity increases sharply, marking the onset of strong optical perturbation. Because $N_c \propto \lambda^{-2}$, longer probe wavelengths require lower carrier densities to reach this regime, making them particularly sensitive to the earliest stages of electron generation. Assuming normal incidence, the instantaneous reflectivity is computed from the Fresnel relation:

$$R(t) = \left|\frac{\sqrt{\varepsilon(\omega,t)}-1}{\sqrt{\varepsilon(\omega,t)}+1}\right|^2, \quad (8)$$

which links the evolving electronic population directly to the macroscopic optical response. The experimentally measured observable is the transient reflectivity change:

$$\Delta R(t) = R(t) - R_0, \quad (9)$$

where R_0 denotes the reflectivity of the unexcited medium, [3], [19]. Because $\varepsilon(\omega,t)$ is explicitly dependent on $N_e(t)$, the shape of $\Delta R(t)$ reflects both the rapid rise associated with multiphoton seeding and avalanche amplification, and the subsequent relaxation governed by recombination and carrier-scattering dynamics. Coupling the nonlinear rate-equation framework with the Drude optical response thus provides a consistent description of how microscopic carrier dynamics translate into macroscopic ultrafast reflectivity signals.

3 Resalts and Discussion

In this section, we present numerical simulations of ultrafast free-carrier generation and the resulting transient optical response in a weakly absorbing wide-bandgap dielectric with properties comparable to water, [2], [3], [10], [19]. Using the nonlinear rate-equation framework introduced in Section 2, we follow the time-resolved evolution of the conduction-band electron density under femtosecond excitation and quantify how the interplay of MPI, avalanche multiplication, and recombination shapes the carrier dynamics. Unless otherwise stated, the simulations are performed for Gaussian pulses with durations of 50-100 fs and excitation wavelengths spanning the visible to near-infrared spectral range (400-1550 nm). By combining the calculated electron density with a Drude-type dielectric response, the model allows the transient reflectivity change to be evaluated and directly related to observables measured in ultrafast pump-probe experiments, [6], [7], [8]. The simulations reveal pronounced wavelength-dependent differences in the efficiency of carrier seeding through MPI and its subsequent amplification through avalanche processes, which in turn strongly influence the magnitude and temporal structure of the optical response.

We begin by examining the temporal evolution of the free-electron density for several representative excitation wavelengths. Figure 1 shows the simulated electron-density dynamics $N_e(t)$ obtained from the rate-equation model for femtosecond excitation in the wavelength range 400-1550 nm at a peak laser intensity of $I_0 = 6 \times 10^{13}$ W cm^{-2}. These wavelengths correspond to multiphoton orders $K = 3, 5, 6,$ and 9, respectively, for a bandgap of $E_g \approx 6.5$ eV. The simulations illustrate how the efficiency of the initial multiphoton seeding and the subsequent avalanche amplification depend strongly on the excitation wavelength.

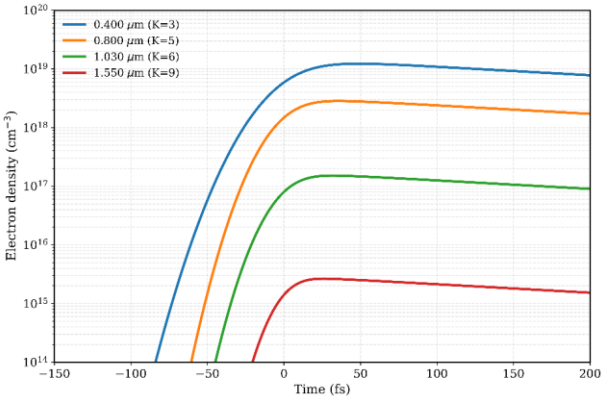

Fig. 1: Temporal evolution of the free-electron density for femtosecond excitation of a water-like dielectric at wavelengths of 400-1550 nm. The curves correspond to multiphoton orders
Source: created by the authors.

The temporal evolution of the free-electron density shown in Figure 1 reflects the strongly nonlinear character of ultrafast ionization dynamics in wide-bandgap dielectric media. Although the overall shape of the curves broadly follows the temporal envelope of the laser pulse, the magnitude and growth rate of the electron population are determined by the interplay between MPI, AI, and carrier recombination. In this framework, MPI provides the initial seed electrons in the conduction band, while AI subsequently amplifies this population through impact processes driven by the laser field. Because MPI is a high-order nonlinear process, its instantaneous rate depends steeply on the laser intensity, scaling approximately as $W_{\mathrm{MPI}} \propto I^K$, where K is the number of photons required to bridge the bandgap. This strong intensity dependence implies that efficient ionization occurs only in the central portion of the pulse where the instantaneous

intensity approaches its maximum value. In the early wings of the pulse, the intensity is too low to drive significant MPI, and the electron density therefore remains essentially negligible. As the pulse approaches its peak, the steep I^K dependence leads to a rapid rise in the electron population, marking the onset of the seeding stage of free-carrier generation, [10], [20]. Once a sufficient seed population has been created, AI becomes increasingly efficient. In this regime, free electrons accelerated by the laser field gain sufficient kinetic energy between collisions to ionize additional bound electrons through impact processes. This multiplication mechanism produces the steep growth of $N_e(t)$ observed around the peak of the laser pulse and typically leads to a slight delay between the maximum of the laser intensity and the maximum electron density. Such a delay is a characteristic signature of the transition from primary PI to impact-driven carrier multiplication and has been reported in numerous studies of femtosecond laser excitation in dielectric and biological media, [2], [3], [10]. A pronounced spectral dependence of the carrier buildup is observed across the considered wavelength range. This behaviour originates from the variation of the multiphoton order K, which determines the efficiency of the initial MPI seeding, [14]. For the shortest wavelength considered, $\lambda = 400$ nm, the bandgap $E_g \approx 6.5$ eV can be bridged by the absorption of three photons, $K = 3$. The relatively low nonlinear order allows efficient generation of seed electrons early in the pulse, enabling strong avalanche multiplication and leading to peak carrier densities of approximately $N_{\mathrm{e,max}} \approx 1.2 \times 10^{19}\,\mathrm{cm}^{-3}$. As the excitation wavelength increases, the multiphoton order rises significantly, which strongly suppresses the MPI rate and reduces the seed population available for avalanche amplification. Consequently, the maximum carrier density decreases to $N_{\mathrm{e,max}} \approx 2.8 \times 10^{18}\,\mathrm{cm}^{-3}$at 800 nm ($K = 5$), $1.5 \times 10^{17}\,\mathrm{cm}^{-3}$ at 1030 nm ($K = 6$), and $2.7 \times 10^{15}\,\mathrm{cm}^{-3}$at 1550 nm ($K = 9$). This systematic reduction illustrates how the increasing multiphoton order strongly limits the efficiency of PI in the near-infrared regime. Following the peak of the laser pulse, the electron density gradually approaches a saturation plateau. This saturation arises from several physical mechanisms acting simultaneously, [10], [21]. First, as the laser intensity decreases after the pulse maximum, both the MPI and AI rates drop rapidly, reducing the generation of new carriers. Second, the recombination term included in the rate equation continuously removes electrons from the conduction band, counteracting further growth of the carrier population. Finally, as the electron density increases, the avalanche growth becomes less efficient because the available energy from the optical field is distributed among an increasing number of carriers. The combined effect of these processes leads to a gradual flattening of the curves and the formation of a quasi-steady carrier population after the pulse. The plateau values, therefore, represent the cumulative number of electrons generated during the laser pulse and effectively determine the strength of the transient optical response of the medium, [9]. Even at identical peak intensities, the strong wavelength dependence of the multiphoton order leads to variations of several orders of magnitude in the final carrier density. The obtained electron density range remains within values commonly reported for femtosecond excitation of dielectric and aqueous systems. It should be noted that a rigorous comparison with breakdown thresholds would necessitate extending the model to include additional processes such as energy transport and post-pulse dynamics, which are not considered in the present ultrafast electronic description. This sensitivity of the electron population to the excitation wavelength plays a crucial role in shaping the optical response of the medium, as will be demonstrated in the following section when the corresponding transient reflectivity signals are analysed.

Having established the wavelength-dependent buildup of the free-electron population, we now examine how this carrier dynamics translate into an observable optical signal. Figure 2 presents the corresponding transient reflectivity change ΔR(t) calculated from the time-dependent electron density using the Drude dielectric response combined with the Fresnel relations at normal incidence. Because the free carriers modify the dielectric permittivity of the medium, the transient reflectivity provides a direct probe of the evolving plasma density during and after the laser pulse. The curves shown in Figure 2 therefore illustrate how the wavelength-dependent carrier populations identified in Figure 1 manifest themselves in the measurable optical response. In particular, the magnitude and temporal structure of ΔR(t) reflect the combined influence of the multiphoton order, avalanche amplification, and the resulting peak electron densities generated during femtosecond excitation.

The curves in Figure 2 exhibit a rapid increase during the central portion of the laser pulse, corresponding to the steep growth of the electron population produced by MPI and subsequent avalanche multiplication. As the electron density increases, the plasma contribution to the dielectric

permittivity becomes stronger, leading to a measurable modification of the surface reflectivity.

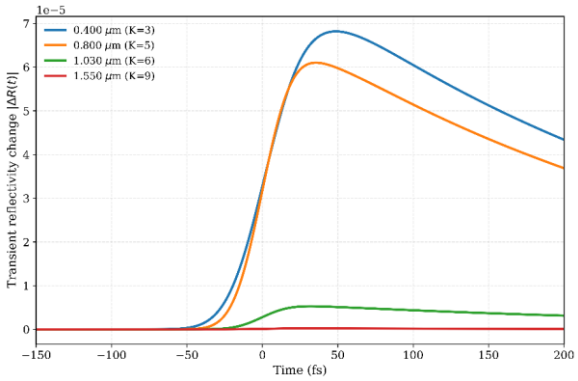

Fig. 2: Transient reflectivity changes for femtosecond excitation of a water-like dielectric at wavelengths of 400-1550 nm. The response is calculated using a Drude model and Fresnel relations at normal incidence (Eq. (9)) for a peak intensity of . Curves correspond to multiphoton orders
Source: created by the authors.

The maximum reflectivity change occurs slightly after the peak of the laser intensity, reflecting the delayed buildup of the electron population associated with AI, [22], [23]. This temporal shift mirrors the behaviour of the carrier-density dynamics and represents a typical signature of ultrafast plasma formation in dielectric media. A pronounced spectral dependence of the optical signal is observed across the considered wavelength range. For the shortest wavelength ($\lambda = 400$ nm), the efficient multiphoton seeding ($K = 3$) and strong avalanche amplification produce the highest carrier density, reaching $N_{\mathrm{e,max}} \approx 1.2 \times 10^{19}\ \mathrm{cm}^{-3}$. This results in the largest reflectivity change, with a peak value of $|\Delta R|_{\max} \approx 6.8 \times 10^{-5}$. At $\lambda = 800$ nm ($K = 5$), the reduced efficiency of MPI lowers the peak electron density to $N_{\mathrm{e,max}} \approx 2.8 \times 10^{18}\ \mathrm{cm}^{-3}$, producing a slightly smaller reflectivity variation of $|\Delta R|_{\max} \approx 6.1 \times 10^{-5}$. A much weaker optical response is obtained for $\lambda = 1030$ nm ($K = 6$), where the peak carrier density decreases to approximately $1.5 \times 10^{17}\ \mathrm{cm}^{-3}$, leading to reflectivity changes on the order of 5×10^{-6}. In the near-infrared regime ($\lambda = 1550$ nm), where the multiphoton order increases to $K = 9$, the ionization process becomes strongly suppressed, and the maximum carrier density remains relatively low, $N_{\mathrm{e,max}} \approx 2.7 \times 10^{15}\ \mathrm{cm}^{-3}$. Consequently, the corresponding reflectivity change is extremely small, with $|\Delta R|_{\max} \approx 2 \times 10^{-7}$. Following the peak of the pulse, the reflectivity signal gradually decays as the electron density decreases due to recombination processes and the diminishing avalanche amplification. Because the recombination time is typically longer than the pulse duration, the optical signal persists after the laser intensity has vanished, producing the slowly decaying tail visible in the curves. This behaviour reflects the relaxation of the laser-generated free-electron plasma and is consistent with transient reflectivity measurements reported for dielectric and biological media, where the optical signal directly traces the temporal evolution of the carrier population, [2], [3], [10]. These results demonstrate that the transient optical response is highly sensitive to the excitation wavelength through its influence on the underlying ionization dynamics. Variations in the multiphoton order lead to substantial differences in the generated carrier density, which in turn produce significant changes in the amplitude of the transient reflectivity signal. It is also important to mention that in the weak-plasma regime considered here, where the electron density remains well below the critical plasma density N_c (see Section 2), the reflectivity perturbation remains small, and the optical response scales approximately with the ratio N_e/N_c, [24]. Since N_c itself depends on the optical frequency, the magnitude of the reflectivity change is influenced both by the generated carrier density and by the excitation wavelength, [25]. As a result, the spectral dependence of the carrier populations obtained in Figure 1 directly translates into the variation of the transient optical signal shown in Figure 2.

To further quantify the wavelength dependence of the excitation dynamics, we now examine two global characteristics of the simulated optical response. Figure 3 summarizes how the threshold conditions for carrier generation and the resulting optical signal vary across the considered spectral range. Panel (a) shows the threshold intensity I_{th} required to produce a detectable plasma response in the medium, while panel (b) presents the corresponding peak transient reflectivity change $|\Delta R|_{\max}$ evaluated at this threshold. By reducing the full temporal dynamics of $N_e(t)$ and $\Delta R(t)$ to these characteristic quantities, the Figure 3 highlights the systematic trends associated with the increasing multiphoton order as the excitation wavelength moves from the visible to the near-infrared region.

Figure 3 shows that the threshold peak intensity I_{th} increases systematically with the excitation wavelength. For excitation at $\lambda = 400$ nm, corresponding to a multiphoton order $K = 3$, the threshold intensity is approximately $2.8 \times 10^{13}\ \mathrm{W\,cm}^{-2}$. As the wavelength increases to 800 nm ($K = 5$), the threshold rises to about $5.0 \times 10^{13}\ \mathrm{W\,cm}^{-2}$. A further increase to 1030 nm ($K = 6$) leads to a threshold of approximately $8.2 \times$

10^{13} W cm^{-2}, while in the near-infrared regime ($\lambda = 1550$ nm, $K = 9$) the required intensity reaches roughly 1.2×10^{14} W cm^{-2}.

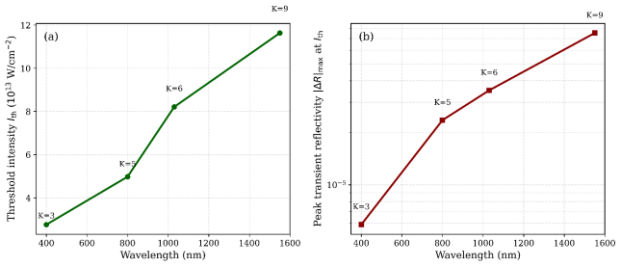

Fig. 3: Wavelength dependence of the excitation threshold and optical response for femtosecond excitation (400-1550 nm) in a water-like dielectric. (a) Threshold intensity . (b) Peak reflectivity change at . Multiphoton orders correspond to
Source: created by the authors.

This monotonic increase reflects the fundamental scaling of MPI with the excitation wavelength, [7]. As the photon energy decreases, a larger number of photons is required to overcome the bandgap of the medium, which significantly reduces the efficiency of PI at a given intensity. Because MPI provides the initial seed population of free carriers that subsequently drives avalanche multiplication, higher laser intensities are required at longer wavelengths to generate enough seed electrons capable of initiating the breakdown process, [6]. The threshold, therefore, marks the transition at which the MPI-generated seed population becomes large enough for AI to dominate the carrier growth during the pulse. Additionally, Figure 3 shows the peak transient reflectivity change evaluated at the threshold intensity. The calculated values reveal a systematic increase in the optical signal with excitation wavelength. At $\lambda = 400$ nm, the peak reflectivity change is approximately $|\Delta R|_{\max} \approx 5.9 \times 10^{-6}$, while at $\lambda = 800$ nm it increases to about 2.4×10^{-5}. For excitation at $\lambda = 1030$ nm, the signal reaches $|\Delta R|_{\max} \approx 4.9 \times 10^{-5}$, and for $\lambda = 1550$ nm it attains a value of approximately 7.5×10^{-5}. It should be noted that these values correspond to the reflectivity evaluated at the wavelength-dependent threshold intensity I_{th}, rather than at a fixed excitation intensity as in Figure 2. Although the threshold intensity increases substantially with wavelength, the optical signal remains clearly observable once the breakdown condition is reached. This behaviour reflects the fact that the threshold corresponds to the onset of avalanche-supported carrier growth, which produces a comparable level of plasma perturbation of the optical properties of the medium across the considered spectral range. Once this regime is reached, the optical response becomes primarily determined by the collective free-carrier contribution to the dielectric function rather than by the details of the initial PI stage. Taken together, these results highlight the dominant role of the multiphoton excitation order in determining the onset of ultrafast plasma formation. Shorter wavelengths favor efficient carrier generation because fewer photons are required to bridge the bandgap, whereas longer wavelengths require significantly higher intensities to compensate for the reduced photon energy and the higher nonlinear order of the ionization process. This interplay between multiphoton seeding and avalanche amplification ultimately governs the wavelength dependence of the LIB threshold in femtosecond laser-dielectric interactions.

4 Conclusion

In this work, we investigated the ultrafast generation of free carriers and the associated transient optical response in water-like dielectric media under femtosecond laser excitation. The carrier dynamics were described using a nonlinear rate-equation model incorporating MPI, avalanche multiplication, and carrier recombination. The resulting time-dependent electron density was subsequently coupled to a Drude dielectric model to evaluate the corresponding transient reflectivity response. The simulations show that the buildup of the free-electron population depends strongly on the excitation wavelength through the multiphoton order. For shorter wavelengths, where fewer photons are required to overcome the bandgap, MPI generates seed electrons efficiently and enables rapid avalanche amplification during the laser pulse. As the wavelength increases toward the near-infrared region, the higher multiphoton order significantly reduces the efficiency of PI. This limits the initial seed population and suppresses the subsequent avalanche-driven growth of the carrier density. The calculated optical response follows the carrier dynamics closely. The transient reflectivity exhibits a rapid increase near the peak of the laser pulse and reaches its maximum slightly afterwards, reflecting the delayed buildup of the electron population associated with avalanche multiplication. The magnitude of the reflectivity change is therefore directly linked to the wavelength-dependent carrier densities produced during the excitation. The analysis of the excitation threshold further clarifies the influence of the wavelength. The peak intensity required to initiate significant carrier multiplication increases systematically from the visible to the near-infrared spectral region. This behaviour reflects the decrease

in photon energy and the corresponding increase in the nonlinear order of the MPI process. Once this threshold is reached, avalanche multiplication leads to a comparable plasma-induced modification of the dielectric response across the investigated spectral range. Overall, the results presented in this study highlight the importance of the excitation wavelength in controlling both the efficiency of ultrafast carrier generation and the resulting optical perturbation in water-like dielectric media. The combined analysis of carrier dynamics and transient optical response provides a consistent physical picture of wavelength-dependent breakdown processes under femtosecond laser excitation.

Acknowledgement:
Authors would like to acknowledge the support received from the Science Fund of the Republic of Serbia, #GRANT 6821, Atoms and (bio) molecules-dynamics and collisional processes on short time scale - ATMOLCOL. Our appreciation also goes to the Serbian Ministry of Education, Science and Technological Development (Agreement No. 451-03-34/2026-03/200122). H. Delibašić Marković would also like to express gratitude to COST Actions CA21159 - "Understanding interaction of light with biological surfaces: possibility for new electronic materials and devices" for their support.

References:

[1] B. Zhang, Z. Wang, D. Tan, and J. Qiu, Ultrafast laser-induced self-organized nano-structuring in transparent dielectrics: fundamentals and applications, PhotoniX, Vol. 4, No. 24, pp. 1–32, 2023, https://doi.org/10.1186/s43074-023-00101-8.

[2] B. C. Stuart, M. D. Feit, S. Herman, A. M. Rubenchik, B. W. Shore, and M. D. Perry, Optical ablation by high-power short-pulse lasers, Journal of the Optical Society of America B, Vol.13, No.2, pp. 459–468, 1996, https://doi.org/10.1364/JOSAB.13.000459.

[3] A. Vogel, J. Noack, G. Hüttman, and G. Paltauf, Mechanisms of femtosecond laser nano-surgery of cells and tissues, Appl. Phys. B, Vol. 81, pp. 1015–1047,2005, https://doi.org/10.1007/s00340-005-2036-6.

[4] M. R. Marks, K. Y. Cheong, and Z. Hassan., A review of laser ablation and dicing of Si wafers, Precision Engineering, Vol. 73, pp. 377–408, 2022, doi: 10.1016/j.precisioneng.2021.10.001.

[5] R. Stoian and M. Sentis, Ultrafast laser-induced processes in dielectrics, J. Phys. D: Appl. Phys., Vol. 42, No. 17, 2009, https://doi.org/10.1117/12.456853.

[6] A. Ashoka, R. R. Tamming, A. V. Girija, H. Bretscher, S. D. Verma, S. D. Yang, C. H. Lu, J. M. Hodgkiss, D. Ritchie, C. Chen, and C. G. Smith, Extracting quantitative dielectric properties from pump-probe spectroscopy, Nature Communications, vol. 13, no. 1, art. no. 1437, pp. 1–9, 2022, https://doi.org/10.1038/s41467-022-29112-y.

[7] L. Qiao, R. R. Pela, and C. Draxl, First-principles approach to ultrafast pump-probe spectroscopy in solids, arXiv preprint arXiv:2509.07612, 2025, https://arxiv.org/pdf/2509.07612.

[8] K. T. Kosma, K. Kaleris, E. Kaselouris, E. Kaniolakis-Kaloudis, S. Petrakis, Y. Orphanos, E. Gagaoudakis, V. Binas, E. Bakarezos, M. Tatarakis, and V. Dimitriou, Pump-probe reflectivity studies of ultrashort laser-induced acousto-mechanical strains in ZnO films, Applied Physics A, Vol.129, No.8, Art. no. 597, pp. 1–11, 2023, https://doi.org/10.1007/s00339-023-06837-1.

[9] N. Brouwer and B. Rethfeld, Excitation and relaxation dynamics in dielectrics irradiated by an intense ultrashort laser pulse, J. Opt. Soc. Am. B, Vol. 31, No. 11, pp. C28–C35, Nov. 2014, https://doi.org/10.1364/JOSAB.31.000C28.

[10] B. Rethfeld, Unified model for the freeelectron avalanche in laserirradiated dielectrics. Phys. Rev. Lett., Vol.92, No.18, 2004, pp.187401-4. https://doi.org/10.1103/PhysRevLett.92.187401

[11] D. Pan, Q. Wan, and G. Galli, The refractive index and electronic gap of water and ice increase with increasing pressure, Nature Communications, Vol.5, Art. No. 3919, pp. 1–6, 2014, https://doi.org/10.1038/ncomms4919.

[12] Y. U. Lee, E. Garoni, H. Kita, K. Kamada, B. H. Woo, Y. C. Jun, S. M. Chae, H. J. Kim, K. J. Lee, S. Yoon, and E. Choi, Strong nonlinear optical response in the visible spectral range with epsilon-near-zero organic thin films, Advanced Optical Materials, Vol.6, No.14, Art. No.1701400, pp. 1-7, 2018, https://doi.org/10.1002/adom.201701400.

[13] Y. I. Jhon, Y. M. Jhon, and J. H. Lee, Broadband ultrafast photonics of two-dimensional transition metal carbides (MXenes), Nano Futures, Vol.4, No.3, Art. No. 032003, pp. 1–24, 2020, https://doi.org/10.1088/2399-1984/aba10a

[14] A. Couairon and A. Mysyrowicz, Femtosecond filamentation in transparent media, Physics

Reports, Vol. 441, No. 2–4, pp. 47–189, 2007, https://doi.org/10.1016/j.physrep.2006.12.005.
[15] N. B. Delone and V. P. Krainov, Multiphoton Processes in Atoms. Berlin, Germany: Springer, 2000, https://doi.org/10.1007/978-3-642-57208-1
[16] L. V. Keldysh, Ionization in the field of a strong electromagnetic wave, Soviet Physics JETP, Vol. 20, No. 5, pp. 1307–1314, 1965, https://inspirehep.net/files/6697e05d52e411291acc8238a780db45 [Access Date: 01/01/2026] .
[17] W. Denk, J. H. Strickler and W. W. Webb, Two-photon laser scanning fluorescence microscopy, Science, Vol. 248, No. 4951, pp. 73–76, 1990, https://doi.org/10.1126/science.2321027.
[18] K. Sokolowski-Tinten and D. von der Linde, Generation of dense electron-hole plasmas in silicon, Physical Review B, Vol. 61, No. 4, pp. 2643–2650, 2000, https://doi.org/10.1103/PhysRevB.61.2643.
[19] S. K. Sundaram and E. Mazur, Inducing and probing non-thermal transitions in semiconductors using femtosecond laser pulses, Nature Materials, Vol.1, No.4, pp. 217–224, 2002, https://doi.org/10.1038/nmat767.
[20] O. Brenk and B. Rethfeld, Electron dynamics in transparent materials under high-intensity laser irradiation, in Laser-Induced Damage in Optical Materials: 2011, Proc. SPIE, vol. 8190, pp. 398–412, Nov. 2011, https://doi.org/10.1117/12.899189.
[21] X. Fang and S. R. Ahmad, Saturation effect at high laser pulse energies in laser-induced breakdown spectroscopy for elemental analysis in water, Laser and Particle Beams, Vol. 25, No. 4, pp. 613–620, 2007, https://doi.org/10.1017/S0263034607000729
[22] D. Wellershoff, J. Hohlfeld, J. Güdde, and E. Matthias, The role of electron–phonon coupling in femtosecond laser damage of metals, Applied Physics A, Vol. 69, No.7, pp. S99–S107, 1999.
[23] A. Vogel and V. Venugopalan, Mechanisms of pulsed laser ablation of biological tissues, Chemical Reviews, Vol. 103, No. 2, pp. 577–644, 2003, https://doi.org/10.1021/cr010379n.
[24] A. Vogel, J. Noack, K. Nahen, D. Theisen, S. Busch, U. Parlitz, D. X. Hammer, G. D. Noojin, B. A. Rockwell, and R. Birngruber, Energy balance of optical breakdown in water at nanosecond to femtosecond time scales, Applied Physics B: Lasers and Optics, Vol. 68, No. 2, pp. 271–280, 1999, https://doi.org/10.1007/s003400050617.
[25] K. Sokolowski-Tinten and D. Von der Linde, Generation of dense electron-hole plasmas in silicon, Physical Review B, Vol. 61, No. 4, p. 2643, 2000, https://doi.org/10.1103/PhysRevB.61.2643.

Contribution of Individual Authors to the Creation of a Scientific Article (Ghostwriting Policy)

The authors equally contributed in the present research, at all stages from the formulation of the problem to the final findings and solution.

Sources of Funding for Research Presented in a Scientific Article or Scientific Article Itself

The research presented in this scientific article was funded by the Science Fund of the Republic of Serbia, Grant No. 6821, Atoms and (Bio)Molecules: Dynamics and Collisional Processes on Short Time Scales (ATMOLCOL). The authors also acknowledge support from the Ministry of Science, Technological Development and Innovation of the Republic of Serbia under Agreement No. 451-03-34/2026-03/200122.

Conflict of Interest

The authors have no conflicts of interest to declare that are relevant to the content of this article.